Biophysical Journal Volume 75 October 1998 1712–1726

Electroreceptor Model of the Weakly Electric Fish *Gnathonemus petersii*. I. The Model and the Origin of Differences between A- and B-Receptors

Jianwei Shuai, Yoshiki Kashimori, and Takeshi Kambara
Department of Applied Physics and Chemistry, The University of Electro-Communications, Chofu, Tokyo 182-8585, Japan

ABSTRACT We present an electroreceptor model of the A- and B-receptors of the weakly electric fish *Gnathonemus petersii*. The model consists of a sensory cell, whose membrane is separated into an apical and basal portions by support cells, and an afferent fiber. The apical membrane of the cell contains only leak channels, while the basal membrane contains voltage-sensitive Ca^{2+} channels, voltage-sensitive and Ca^{2+}-activated K^+ channels, and leak channels. The afferent fiber is described with the modified Hodgkin-Huxley equation, in which the voltage-sensitive gate of the K^+ channels is a dynamic variable. In our model we suggest that the electroreceptors detect and process the information provided by an electric organ discharge (EOD) as follows: the current caused by an EOD stimulus depolarizes the basal membrane to a greatly depolarized state. Then the release of transmitter excites the afferent fiber to oscillate after a certain time interval. Due to the resistance-capacitance structure of the cells, they not only perceive the EOD intensity, but also sense the variation of the EOD waveform, which can be strongly distorted by the capacitive component of an object. Because of the different morphologies of A- and B-cells, as well as the different conductance of leak ion channels in the apical membrane and the different capacitance of A- and B-cells, A-receptors mainly respond to the EOD intensity, while B-receptors are sensitive to the variation of EOD waveform.

INTRODUCTION

The weakly electric fish *Gnathonemus petersii* emits pulse-type electric organ discharges (EODs) with an electric organ in its caudal peduncle. During each discharge an electrical field is built up around the fish's body, which is perceived by the sender fish and by other electric fish nearby. The electroreceptor organs of *G. petersii* are of three distinct types: mormyromasts, knollenorgans, and ampullary organs (Bennett, 1965). Mormyromasts are the only type of electroreceptor organs used to sense the self-emitted EODs during active electrolocation.

Each mormyromast organ contains an outer and an inner sensory chamber (Szabo and Wersall, 1970; Bell et al., 1989). The outer sensory chamber is connected to the outside surface of the skin by a plug of loosely packed epithelial cells and is connected to the lower sensory chamber by a canal. There are two types of mormyromast sensory cells: A-cells and B-cells. Each sensory cell is contacted by an afferent fiber. Impulse generation in the afferent fiber is induced by transmitter release, which occurs when the basal membrane potential of the sensory cells is depolarized by an EOD. The spike latencies of the afferent fiber encode the amplitude and/or distortion of the EOD waveform (Szabo and Hagiwara, 1967; Bell, 1990; Hall et al., 1995; von der Emde and Bleckmann, 1997).

During active electrolocation, when an object with electric properties different from those of the surrounding water comes close, the fish's electric field will be distorted and the pattern of voltage gradients at the mormyromast electroreceptors is changed. Animate objects, like other fishes, plants, or insect larvae, have a complex impedance consisting of a resistive and a capacitive component (Schwan, 1963; Heiligenberg, 1973). Depending on their electric properties, electrolocation objects can alter the amplitude of the local EOD and/or its waveform. EOD amplitude depends on the impedance of the object under investigation: an impedance higher than that of the water decreases local EOD amplitudes, while objects with a lower impedance than the water increase local EOD amplitudes (Heiligenberg, 1973). Capacitive objects cause alterations of the waveform of the locally received EOD owing to frequency-dependent amplitude attenuation and phase shift of the EOD (Heiligenberg, 1973; Bastian, 1986; von der Emde, 1990).

A-receptors are pure amplitude coders (Bell, 1990; von der Emde 1990; von der Emde and Bleckmann, 1992a, b). EOD waveform distortions, which are caused only by capacitive objects, slightly alter the response of A-receptors in a similar way, as does a reduction in stimulus amplitude (von der Emde and Bleckmann, 1992a, b). B-receptors respond similarly to A-receptors with respect to stimulus amplitude changes (Bell, 1990; von der Emde and Bleckmann, 1992a, b; 1997). In contrast to A-receptors, however, B-receptors are extremely sensitive to EOD waveform distortions (von der Emde and Bleckmann, 1992a,b, 1997). Their afferent fibers respond to a distorted EOD with shorter latency and an increased number of spikes per burst, even if the EOD amplitude has been kept constant. Thus,

Received for publication 2 March 1998 and in final form 8 June 1998.

Address reprint requests to Dr. Yoshiki Kashimori, Department of Applied Physics and Chemistry, University of Electro-Communications, Chofu, Tokyo 182-8585, Japan. Tel.: 81-424-43-5470; Fax: 81 424 89 9748; E-mail: kashi@nerve.pc.uec.ac.jp.

Dr. Shuai's current address: Department of Biomedical Engineering, Applied Neural Control Laboratory, Case Western Reserve University, Cleveland, Ohio 44106 USA.

0006-3495/98/10/1712/15 $2.00

they respond to an EOD phase-shift as if EOD amplitude had increased. As a result, mormyrids unequivocally discriminate between resistive and capacitive objects during electrolocation (von der Emde and Bell, 1994). The fish can also discriminate between objects of different capacitive values (von der Emde, 1993). Waveform tuning of electroreceptors of *G. petersii* is discussed in detail by von der Emde and Bleckmann (1997). Experiments with computer-generated stimuli reveal that the strong sensitivity of B-receptors to EOD waveform distortions cannot be attributed to any of seven waveform parameters tested (von der Emde and Bleckmann, 1997). It is still unclear to which parameter of the distorted EOD B-receptors are sensitive.

In this series of papers we are concerned with the nonlinear mechanism of information processing by A- and B-receptors, and try to answer the following questions. What are the microscopic neural dynamics of A- and B-receptors? What differences cause A-receptors to be amplitude coders while B-receptors are waveform coders? What parameters of the distorted EOD are B-receptors sensitive to? Why are B-receptors more sensitive to EODs than A-receptors?

To systematically clarify the microscopic origins of most of the observed properties of A- and B-receptors of weakly electric fish *G. petersii*, we present a model that consists of a sensory cell perceiving the EOD and an afferent nerve fiber innervating the cell. The system considered is of active electroreception. Due to its resistance-capacitance structure, the sensory cell perceives not only the EOD amplitude, but also the variation of the EOD waveform. With the model, we show that the functional differences between A- and B-receptors are caused by differences in morphology of the sensory cells, as well as by differences of physical properties of the sensory cells, i.e., the different conductance of the leak ion channels of the apical membrane and the different capacitance of A- and B-cells. As a result, A-receptors mainly respond to the EOD amplitude, while B-receptors are sensitive to the variation of the EOD waveform. These differences also cause B-receptors to be more sensitive to stimuli than A-receptors. In the present paper we mainly concentrate on the investigation of the dynamics of the electroreceptor. In the second paper (Shuai, Kashimori, Kambara, and von der Emde, manuscript in preparation), we will discuss the responses of A- and B-receptor models to EODs distorted by various resistive and capacitive objects, to phase-shifted EODs, and to single periodic sinusoidal stimuli.

MODELS

Kashimori et al. (1996) described a general model of P- and T-electroreceptor cells in the wavetype electric fish, *Eigenmannia*. In the model, the ionic currents across the apical and basal membrane of the receptor cell and the support cells are taken into account. Leak channels of Na^+, K^+, and Cl^- are included in the apical and basal membranes that contribute mainly to the determination of the resting potential of the sensory cell. The basal membrane of the cell has voltage-sensitive Ca^{2+} channels and Ca^{2+}-activated K^+ channels that are responsible for their regenerative voltage responses.

In the present sensory cell model, the contribution of supporting cells is ignored due to their high resistance. For simplicity, the assumption of a unified effective conductance has been used for the leak channels of Na^+, K^+ and Cl^- in the basal and apical membranes, as shown in Fig. 1. The cell membrane is separated by the supporting cells into apical and basal membranes. While the apical membrane contains only the effective leak channels, the basal membrane contains voltage-sensitive Ca^{2+} channels, voltage-sensitive and Ca^{2+}-activated K^+ channels, and effective leak channels.

The afferent fiber is described by the modified Hodgkin-Huxley equations in which the voltage-sensitive gate of the K^+ channels is a dynamic variable. Spike generation in the afferent fiber is induced by transmitter release at the synapse, which occurs when the basal membrane of the sensory cell is depolarized.

Sensory cell model

The equivalent circuit model of a sensory cell system is given in Fig. 2. The electric current density I_A in the apical membrane of the cell consists of the displacement current caused by the capacitance of the apical membrane and the ionic current flowing through the effective leak channel, i.e.,

$$I_A = C_1 \frac{d\Phi_A}{dt} + g_0(\Phi_A - \Phi_0) \tag{1}$$

where C_1 is the capacitance of the unit area of apical membrane, Φ_A is the potential of the apical membrane, g_0 is the conductance of the effective leak ion channels of the unit area in the apical membrane, and Φ_0 is the equilibrium potential of leak channels.

The electric current density I_B in the basal membrane consists of the capacitive displacement current and ionic currents flowing through the Ca^{2+}, K^+, and leak channels:

$$I_B = C_2 \frac{d\Phi_B}{dt} + I_{Ca} + I_K + I_L \tag{2}$$

with

$$\begin{aligned} I_{Ca} &= g_{Ca}^B(\Phi_B - \Phi_{Ca}) \\ I_K &= g_K^B(\Phi_B - \Phi_K) \\ I_L &= g_L^B(\Phi_B - \Phi_L) \end{aligned} \tag{3}$$

where C_2 is the capacitance of the unit area of basal membrane; Φ_B is the potential of the basal membrane; g_{Ca}^B, g_K^B, and g_L^B are conductance of Ca^{2+}, K^+, and leak channels of the unit area in the basal membrane, respectively; and Φ_{Ca}, Φ_K, and Φ_L are the equilibrium potentials of ion Ca^{2+}, K^+, and leak channels across the basal membrane, respectively.

For the equivalent circuit, there are two conservation laws as

$$\begin{aligned} S_1 I_A - S_2 I_B &= 0 \\ \Phi_A + \Phi_B &= V_{stim} \end{aligned} \tag{4}$$

where S_1 and S_2 are the areas of apical and basal membranes, respectively, and V_{stim} is the stimulation potential applied to the cell.

Substituting Eqs. 1–3 into Eq. 4, the equation for Φ_B can be obtained as

$$\begin{aligned} C_0 \frac{d\Phi_B}{dt} = S_1 C_1 \frac{dV_{stim}}{dt} + S_1 g_0(V_{stim} - \Phi_B - \Phi_0) \\ - S_2(I_{Ca} + I_K + I_L) \end{aligned} \tag{5}$$

with $C_0 = C_1 S_1 + C_2 S_2$.

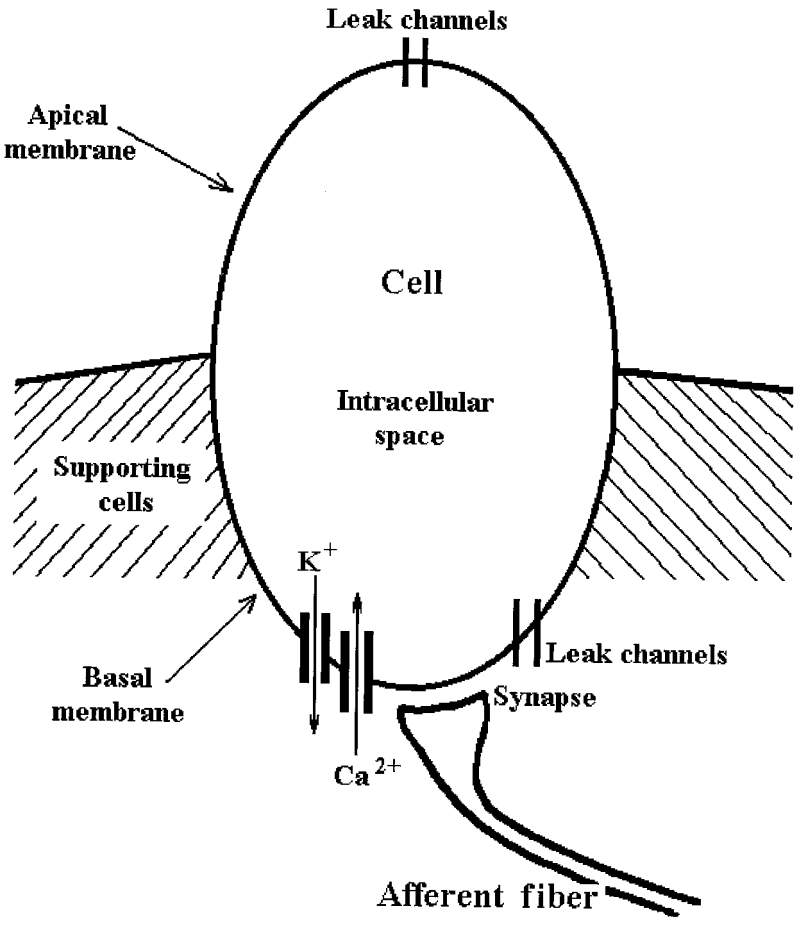

FIGURE 1 Schematic representation of a mormyromast electroreceptor of weakly electric fish. Supporting cells divide the receptor cell membrane into apical and basal membranes. The apical membrane has only leak channels. The basal membrane has Ca^{2+} and K^+-active channels besides the leak channels.

In the present model, the Ca^{2+} channel of the basal membrane that allows extracellular Ca^{2+} to enter the cell is voltage-sensitive, i.e., $g^B_{Ca} = \bar{g}^B_{Ca} d(\Phi_B)$. The K^+ channel that allows intracellular K^+ to leave the cell contains a voltage-sensitive activation gate $f(\Phi_B)$ and a free intracellular $[Ca^{2+}]$-activated gate $g([Ca^{2+}])$, i.e., $g^B_K = \bar{g}^B_K fg$. The opening of the d-gate and f-gate is assumed to take place very fast. Then they are treated reasonably as the nondynamic variables and can be approximated by the steady-state values d_∞ and f_∞, which are sigmoid functions of basal membrane potential. These function can be expressed by the Boltzmann equation (Rorsman and Trube, 1986; Chay, 1990b) as

$$d_\infty = \frac{1}{1 + \exp[-(\Phi_B - V_d)/S_d)]}$$
$$f_\infty = \frac{1}{1 + \exp[-(\Phi_B - V_f)/S_f)]} \quad (6)$$

where S_d, S_f and V_d, V_f are the steepness factors and the half-maximal activation potentials, respectively. The $[Ca^{2+}]$-activated gate g is written as

$$g = \frac{1}{1 + \ln(1/[Ca^{2+}]_{sub})}. \quad (7)$$

Here we consider that the $[Ca^{2+}]$-activated gate g of K^+ channels depends only on the compartmentalized calcium ion concentration $[Ca^{2+}]_{sub}$ in the submembrane space (Chay, 1990a, 1993).

The free intracellular calcium concentration $[Ca^{2+}]_{sub}$ in the submembrane space is treated as a dynamic variable in the model, and its changes with time arise from the following two terms: the influx of extracellular calcium ions into the cell through the voltage-sensitive calcium channel and the efflux of free intracellular Ca^{2+} ions from the submembrane space to the extracellular medium by the pump action and to the intracellular medium by absorption. We thus have

$$\frac{d[Ca^{2+}]_{sub}}{dt} = \frac{-\alpha I_{Ca} - \beta[Ca^{2+}]_{sub}}{\tau} \quad (8)$$

where β is the rate constant for the efflux pump and intracellular absorption of calcium ions; $\alpha = 3/(4\pi r^3 F)$, where F is the Faraday constant and r the effective radius of the cell. τ is a measure of how fast the free calcium concentration $[Ca^{2+}]_{sub}$ changes in the submembrane space. We assume that τ is a function of Φ_B,

$$\tau = \tau_{min} + \frac{\tau_0}{1 + \exp[-(\Phi_B - V_\tau)/S_\tau]}. \quad (9)$$

Note that $\tau = \tau_{min}$ when $\Phi_B = -\infty$ and $\tau = \tau_{min} + \tau_0$ when $\Phi_B = \infty$. S_τ and V_τ are the steepness factor and the half-maximal activation potential, respectively. Equation 9 is derived based on the assumption that the Ca^{2+} ions in the submembrane space of the cell move faster when the depolarized potential of the cell is low. In pancreatic β-cells or HIT cells, the experiments have shown that calcium ions can oscillate even though the calcium ion channels are closed (Penner and Neher, 1988; Lund et al., 1991; Prentki et al., 1988). This implies that the intracellular calcium ions are not always free and are distributed heterogeneously. There are some calcium ion compartments or stores in the cell (Velasco and Petersen, 1987; Chay, 1990a, 1993). The $[Ca^{2+}]$-activated gate g of K^+ channels depends on the compartmentalized calcium ion concentration in the submembrane space that corresponds to the observable concentration of free intracellular calcium ions. Large depolarization of the cell causes a large inward current carried by calcium ions; in this case, many calcium ions flow into the cell rapidly. Although the total calcium concentration in the

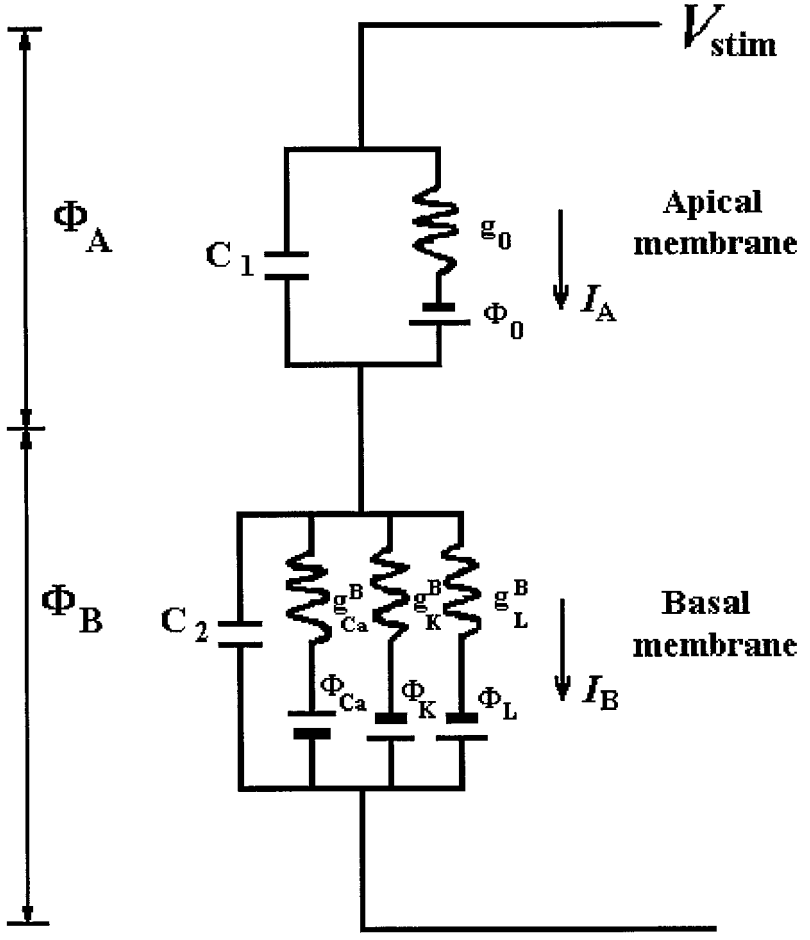

FIGURE 2 The equivalent circuit of the receptor model. Φ_A and Φ_B are the potentials of the apical and basal membranes of the cell, respectively; C_1 and C_2 are the capacitances of the unit area of apical and basal membranes, respectively; g_0 is the conductance of the leak ion channels of the unit area in the apical membrane; Φ_0 is the equilibrium potential of leak channels; g^B_{Ca}, g^B_K, and g^B_L are conductances of Ca^{2+}, K^+, and effective leak channels of the unit area in the basal membrane, respectively; Φ_{Ca}, Φ_K, and Φ_L are the equilibrium potentials of ion Ca^{2+}, K^+, and mixed leak channels across the basal membrane, respectively. The arrows attached to I_A and I_B indicate the positive directions of relevant current.

cell increases greatly, most of the calcium ions are driven into compartments within the cell. Therefore, the number of free intracellular calcium ions in the submembrane space is changed slowly, i.e., the rate of change τ of free intracellular calcium ions in the submembrane space is small. In contrast, for small depolarization, the calcium ions move into the cell slowly, so that more calcium ions remain in the submembrane space of the cell, which activates the gate g of K^+ channels. That is, τ becomes large.

Afferent fiber model

Spike generation in the afferent nerve fiber is induced by transmitter release, which occurs when the basal membrane potential of the cell is depolarized sufficiently (Sanchez and Zakon, 1990; Kashimori et al., 1996). To calculate the impulse trains in the afferent fiber, the modified Hodgkin-Huxley equations were used. As shown by Hodgkin and Huxley (1952), the membrane potential V at the axon terminal is determined by

$$C\frac{dV}{dt} = -g_{Na}m^3h(V - V_{Na}) - g_K n^4(V - V_K) - g_L(V - V_L) + I_{ps} \tag{10}$$

where C is the membrane capacitance of the afferent fiber, g_{Na} and g_K are the maximum conductance of the active Na^+ and K^+ channels, respectively, when all channels are open; g_L is the conductance of leak ion channels; m, h, and n are the gating parameters; and V_{Na}, V_K, and V_L are the equilibrium potentials of Na^+, K^+, and leak ions, respectively.

The gating variables m, h, and n are time-dependent such that the opening of the gates takes place by a simple two-state mechanism. If the opening and closing of channels are very fast, the probability in the open state can be replaced by its steady-state expression. In the present model, the usual time dependencies of m and h in the Hodgkin-Huxley equations are assumed to be replaced by their steady-state values m_∞ and h_∞. The probability, n, is a dynamic variable whose value can be obtained by solving the following first-order equation:

$$\frac{dn}{dt} = \frac{n_\infty - n}{\tau_n}. \tag{11}$$

Let y stand for m, h, and n; then the explicit expressions for m_∞, h_∞, and n_∞ can be written as

$$y_\infty = \frac{\alpha_y}{\alpha_y + \beta_y} \tag{12}$$

where α_y and β_y are the activation and deactivation rates of the two-state mechanism, respectively, and expressed as (Chay, 1985)

$$\alpha_m = 0.1\frac{V + 25}{1 - \exp[-(V + 25)/10]}$$

$$\beta_m = 4\exp\left(-\frac{V + 50}{18}\right)$$

$$\alpha_h = 0.07\exp\left(-\frac{V + 50}{20}\right)$$

$$\beta_h = \frac{1}{1 + \exp[-(V + 25)/10]}$$

$$\alpha_n = 0.01\frac{V + 20}{1 - \exp[-(V + 20)/10]}$$

$$\beta_n = 0.125 \exp\left(-\frac{V + 30}{80}\right) \quad (13)$$

The relaxation time constant of the n-gate is expressed in terms of α_n and β_n as

$$\tau_n = \frac{\tau_{n0}}{\alpha_n + \beta_n} \quad (14)$$

The postsynaptic current I_{ps} in Eq. 10 is induced by the neural transmitter released from the presynaptic membrane of the sensory cell. The magnitude of I_{ps} is proportional to the intensity of released transmitter, which is determined by the Ca^{2+} current I_{Ca} across the basal membrane. Following Kashimori et al. (1996), the relation of I_{ps} to I_{Ca} is written as a sigmoid function

$$I_{ps} = \frac{w}{1 + \exp[-(I_{Ca} - \theta)/\epsilon]} \quad (15)$$

where I_{Ca} is given by Eq. 3, w is the strength of synaptic connection, θ is the threshold value for the transmitter release, and ϵ is the parameter determining the rising of the sigmoid curve. When $I_{Ca} > \theta$, a large stimulus current I_{ps} is induced.

RESULTS AND DISCUSSION

In the present paper, first we discuss the dynamics of the sensory cell and the afferent fiber models in detail. Stimulated by an EOD, the sensory cell is excited to a large depolarization state with a duration of ~10 ms. Thus, a high calcium ion current is achieved with a duration of ~10 ms. The current causes the release of transmitter to the afferent fiber. The afferent fiber is then driven to fire after a certain time interval. One of the purposes of the present study is to clarify the origin of the functional differences between A- and B-receptors. Experimental results of receptors responding to a square wave stimulus (Bell, 1990) are considered based on the present model. We use the parameter values listed in Tables 1 and 2 for the computation. The parameter values of the equilibrium potentials and the conductance of ion channels are typical ones. For the other parameters, the reasons why we adopted the values listed in the tables are given at suitable points in the following three subsections. It is noted in Table 1 that, besides the different morphology of the A- and B-cells, the conductance of the leak channels of the apical membrane and the capacitance of the apical membrane are different in A- and B-cells.

TABLE 1 Different parameter values used for the models of A- and B-cells

Cell	Parameter	Equation	Value	Unit
	$C_1 = C_2 = C_A$	5	3.0×10^{-2}	$\mu F/cm^2$
A-cell	S_1/S_2	5	0.1	
	g_0	5	3×10^3	$\mu S/cm^2$
	$C_1 = C_2 = C_B$	5	2.5×10^{-3}	$\mu F/cm^2$
B-cell	S_1/S_2	5	10.0	
	$g_0(B)$	5	3×10	$\mu S/cm^2$

TABLE 2 Parameter values used for the A- and B-receptor models

Parameter	Equation	Value	Unit
Φ_0	3	−70.0	mV
Φ_{Ca}	3	100.0	mV
Φ_K	3	−80.0	mV
Φ_L	3	−70.0	mV
$\bar{g}^B_{Ca}$	3	7.8×10^4	$\mu S/cm^2$
$\bar{g}^B_K$	3	4.56×10^5	$\mu S/cm^2$
g^B_L	3	8.4×10^3	$\mu S/cm^2$
S_d	6	10.0	mV
V_d	6	−10.0	mV
S_f	6	10.0	mV
V_f	6	−16.0	mV
α	8	10^{-7}	mM/mA
β	8	1.7457	
τ_{min}	9	0.009	s
τ_0	9	440.0	s
S_τ	9	0.1	mV
V_τ	9	−5.6	mV
C	10	1.0	$\mu F/cm^2$
g_{Na}	10	4×10^5	$\mu S/cm^2$
g_K	10	3×10^5	$\mu S/cm^2$
g_L	10	10^3	$\mu S/cm^2$
V_{Na}	10	100	mV
V_K	10	−80	mV
V_L	10	−70	mV
τ_{n0}	14	10^4	s
w	15	24.0	μA
θ	15	−4900	$\mu A/m^2$
ϵ	15	40.0	$\mu A/m^2$

Dynamics of the sensory cell

In the sensory cell model, we propose that the EOD stimulus drives the cell to a large depolarized state with a duration of ~10 ms. Here we show how the model can achieve this dynamical property.

First, we consider the dynamical properties of the current density in Eq. 5, i.e., $-S_1 g_0(\Phi_B + \Phi_0) - S_2(I_{Ca} + I_K + I_L)$, for a fixed value of $[Ca^{2+}]_{sub}$. Because the values of $g_0 S_1/S_2 = 300\ \mu S/cm^2$ for both A- and B-cells, we consider the following current density I_c:

$$I_C = -300(\Phi_B + \Phi_0) - [\bar{g}^B_{Ca} d_\infty(\Phi_B - \Phi_{Ca}) + \bar{g}^B_K f_\infty g(\Phi_B - \Phi_K) + g^B_L(\Phi_B - \Phi_L)] \quad (16)$$

In Fig. 3 the current density I_c versus the basal membrane potential Φ_B are plotted for different fixed values of Ca^{2+} concentration. The simulation shows that there are two stable fixed points ($I_c = 0$) when $[Ca^{2+}]_{sub} < 0.01867$ mM. From $I_c = 0$ and $d[Ca^{2+}]_{sub}/dt = 0$ (Eq. 8), the resting equilibrium state of the cell is obtained with $\Phi^r_B = -52$ mV and $[Ca^{2+}]^r_{sub} = 0.01$ mM. When 0.01 mM $< [Ca^{2+}]_{sub} <$ 0.01867 mM, one stable fixed point (Φ^h_B) corresponds to the

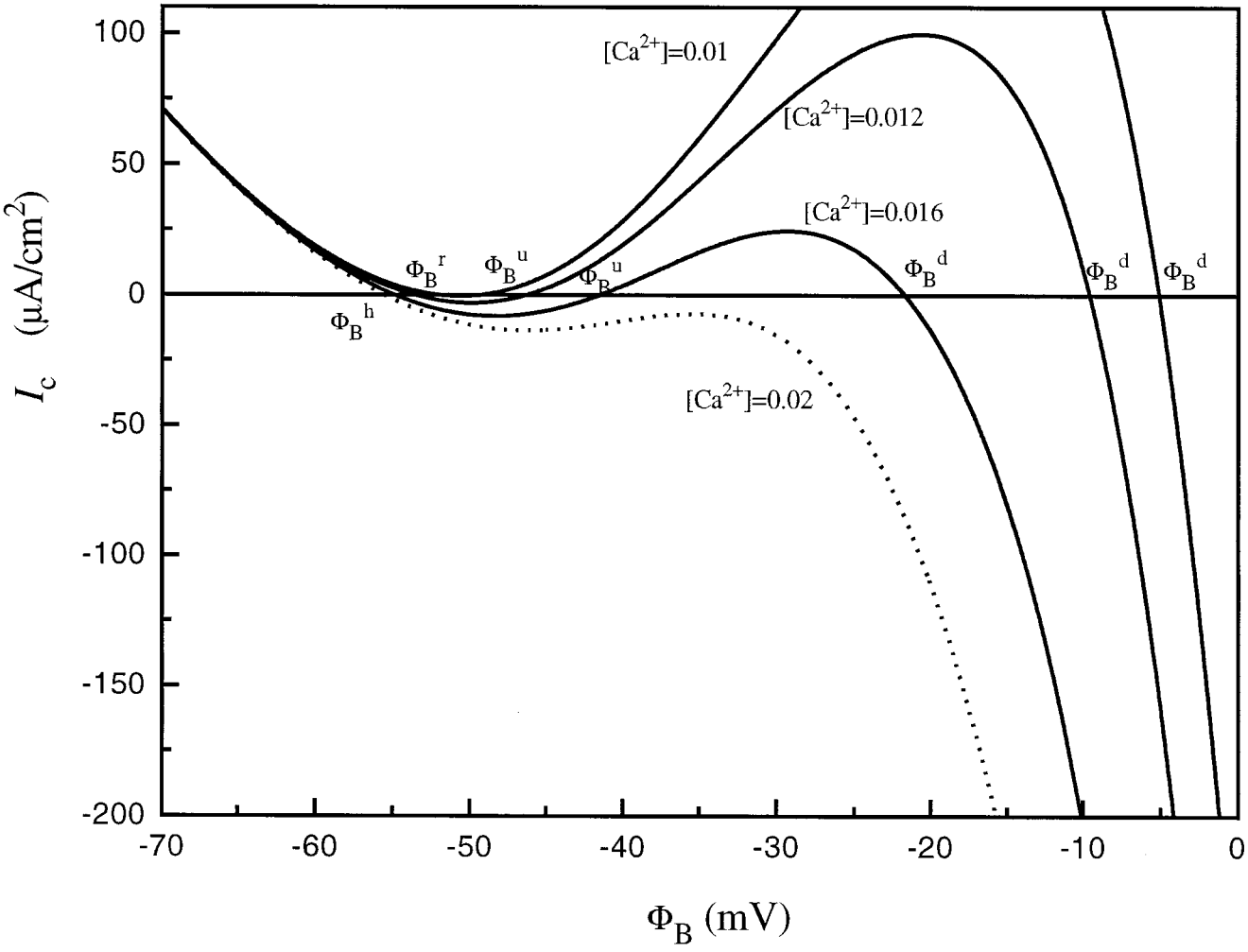

FIGURE 3 The curves of current I_c through the basal membrane versus the basal potential Φ_B for different fixed $[Ca^{2+}]_{sub}$ (0.01, 0.012, 0.016, and 0.02 mM). Φ_B^r is the resting equilibrium state when $[Ca^{2+}]_{sub} = 0.01$ mM; Φ_B^d is the greatly depolarized state. The unstable fixed points Φ_B^u separate the attraction regions to the resting and depolarized ones.

hyperpolarized state, which is quite near the resting equilibrium state Φ_B^r, and another point corresponds to the greatly depolarized state Φ_B^d. Corresponding to the two fixed points there are two stable attracting regions that are separated by the unstable fixed point Φ_B^u, i.e., the resting attraction region with the attractor point Φ_B^h and the exciting attraction region with the attractor point Φ_B^d. However, $[Ca^{2+}]_{sub}$ is a dynamical variable determined by Eq. 8. Once the sensory cell is depolarized, $[Ca^{2+}]_{sub}$ increases gradually. When $[Ca^{2+}]_{sub} > 0.01867$ mM, the Ca^{2+}-activated gate g becomes so large that the outward currents exceed the inward Ca^{2+}-current. As shown in Fig. 3 with the dotted line, the greatly depolarized state becomes unstable and then only the hyperpolarized state Φ_B^h is stable.

Fig. 4 shows the response of the model of an A-cell to a half-period positive sine stimulus (Fig. 4 *a*) given by $A \sin(\omega t)$ with $A = 5.0$ mV and $\omega = 1000\ s^{-1}$. A similar result can be obtained for the model of a B-cell. With a large enough stimulus, the potential of the cell is depolarized (Fig. 4 *b*). When the depolarized potential exceeds the unstable fixed point, i.e., $\Phi_B > \Phi_B^u$, the cell is driven to the exciting attractor region from its resting attractor region. Once it enters this region, the cell automatically becomes greatly depolarized. Because of the short duration of the positive sinusoidal signal (0.5 ms), the calcium ion concentration change is small. Our simulation results show that when $t = 0.5$ ms, $[Ca^{2+}]_{sub}$ becomes 0.01034 mM. At this small calcium ion concentration, the stable depolarized potential of the basal membrane becomes -5.78 mV. The inward calcium ion current density I_{Ca} increases to 4982 μA/cm^2 from its resting equilibrium current density 175.0 μA/cm^2. Although many calcium ions move into the cell during the greatly depolarized state, the free intracellular calcium ion concentration in the submembrane space increases very slowly because most of the calcium ions move rapidly into the interior of the cell; then the greatly depolarized potential decreases very slowly. We adjusted the values of parameters τ_{min}, τ_0, V_τ, and S_τ in Eq. 9 as shown in Table 2 so that the greatly depolarized state could be maintained for ~10 ms. However, the gradual increase of

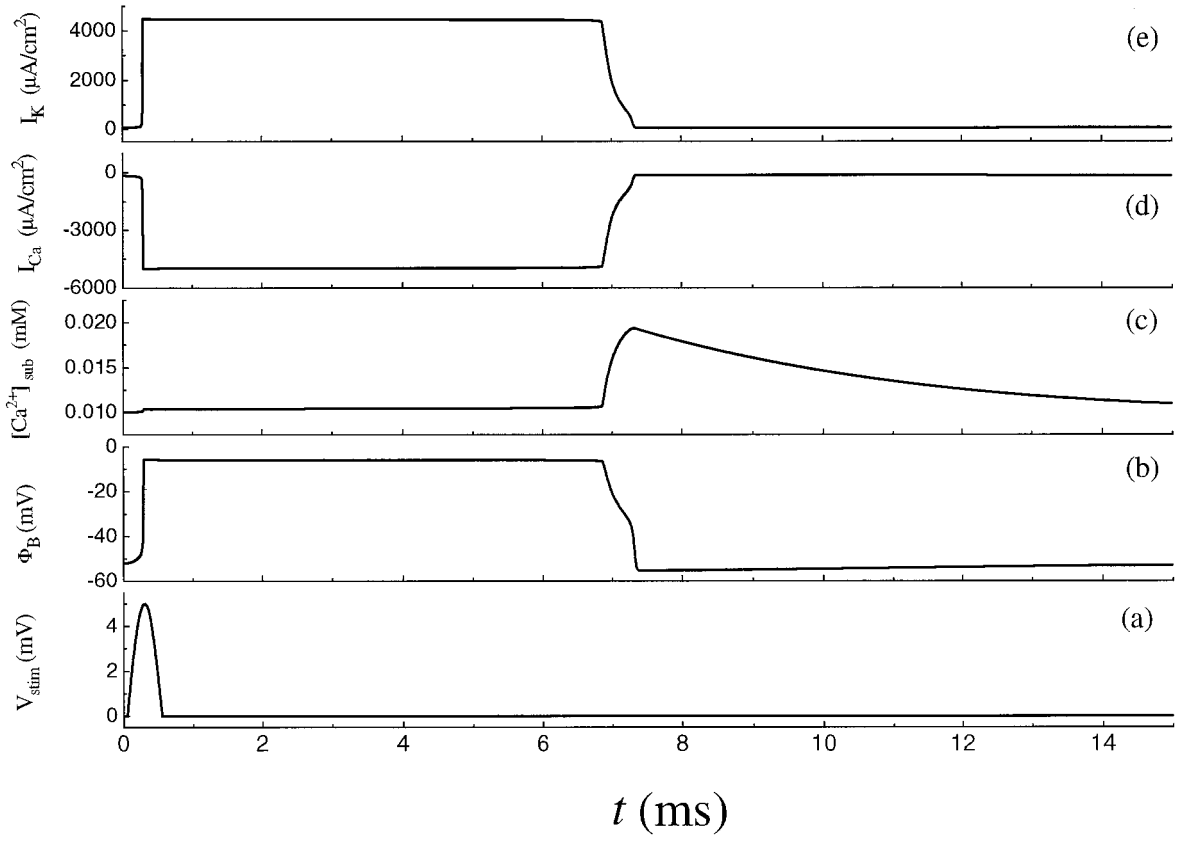

FIGURE 4 The response properties of the A-cell model stimulated by a half period positive sinusoidal stimulus given by $A \sin(\omega t)$ with $A = 5$ mV and $\omega = 1000\ s^{-1}$. (*a*) Stimulus; (*b*) basal membrane potential Φ_B; (*c*) free calcium concentration in the submembrane space of the cell; (*d*) inward calcium current I_{Ca}; (*e*) outward K^+ current I_K.

$[Ca^{2+}]_{sub}$ causes the depolarization to decrease which, in turn, causes $[Ca^{2+}]_{sub}$ to increase more. When the basal membrane potential decreases to -6.2 mV, the relaxation time τ becomes small enough, and consequently $[Ca^{2+}]_{sub}$ and the membrane potential change rapidly. When $[Ca^{2+}]_{sub}$ becomes larger than 0.01867 mM, the Ca^{2+}-activation gate g becomes so large that the outward current exceeds the inward current, and the greatly depolarized state becomes unstable. As a result, the potential of the cell returns to the hyperpolarized state Φ_B^h in the resting attractor region. Then the inward Ca^{2+} current becomes small again. The free Ca^{2+} with high concentration in the submembrane space of the cell is pumped out. After a transient process, the cell gradually goes back to the resting equilibrium state.

Larger stimulus amplitude A induces the transition from the resting equilibrium state to the greatly depolarized state in a shorter time, which causes a smaller increase of $[Ca^{2+}]_{sub}$. The smaller increase of $[Ca^{2+}]_{sub}$ causes a higher depolarized potential of the basal membrane with a longer duration. As a result, a larger calcium ion inward current with longer duration is achieved. In Fig. 5 the maximum difference between the largest depolarized potential and the resting equilibrium potential, i.e., $\Delta\Phi_{Bmax} = \Phi_{Bmax}^d - \Phi_B^r$, is shown as a function of the stimulus amplitude A, together with the curve of the duration of the greatly depolarized state. Here, the greatly depolarized state is defined as the state in which the potential of the basal membrane is larger than -7.0 mV.

Dynamics of the afferent fiber

Our model of an afferent fiber is based on the Chay model (Chay, 1985; Fan and Chay, 1994) which is described by three differential equations. As two bifurcation parameters are varied, a three-variable model can lead to an enormously complex bifurcation structure, including several types of chaos. In the Chay model, the calcium concentration is a slowly varying dynamic variable that generates bursting, while the gating kinetics variable of K^+ channels is a voltage- and time-dependent fast varying dynamical variable that generates the spikes. The third dynamical variable is the membrane potential V, which is a variable depending on both the calcium concentration and the gating kinetics variable. To obtain the oscillation behavior in our model, we simplify the Chay model to two differential equations. In the present model, the fast gating kinetics variable of the K^+ channels is maintained. The values of the parameters appearing in Eq. 13 are the same as those used in the Chay model. In the Chay model, the basic time scale is millisec-

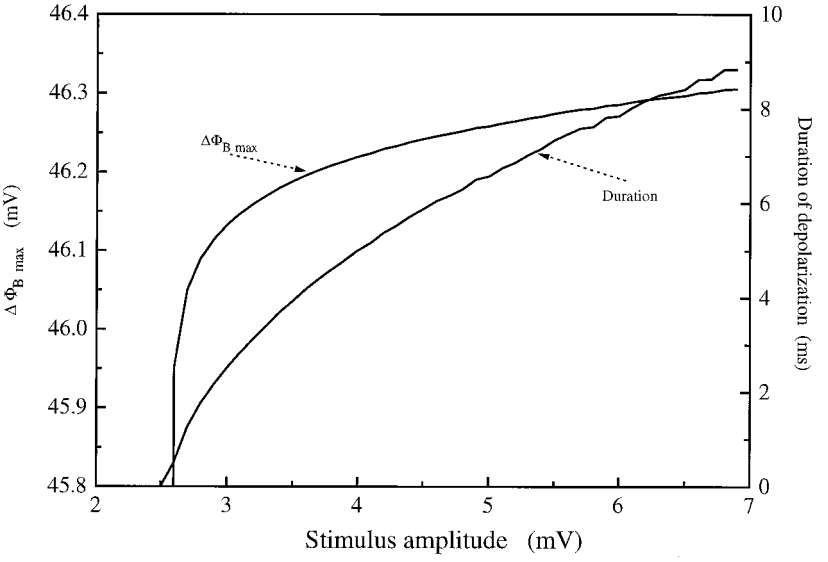

FIGURE 5 The difference $\Delta\Phi_{Bmax}$ between the maximum depolarized potential and the resting equilibrium potential of the basal membrane $\Delta\Phi_{Bmax} = \Phi^{d}_{Bmax} - \Phi^{r}_{B}$ and the duration of greatly depolarized state as functions of the amplitude of the stimulus $A\sin(\omega t)$ with $\omega = 1000\ s^{-1}$. Here the greatly depolarized state is defined as its basal membrane potential is > -7.0 mV.

ond, while the microsecond scale is required for the dynamics in A- and B-receptors. Therefore, we modify the values of the conductance and the equilibrium potentials of the three kinds of channel gates, and the relaxation time τ_{n0} of *n*-gate.

To discuss the dynamics of the afferent fiber model in detail, we let $I_{ps} = 20\ \mu$A. The simulation results are shown in Fig. 6. When the afferent fiber is stimulated by a constant current I_{ps}, the membrane potential V of the afferent fiber is depolarized gradually. Then the voltage-sensitive Na^+

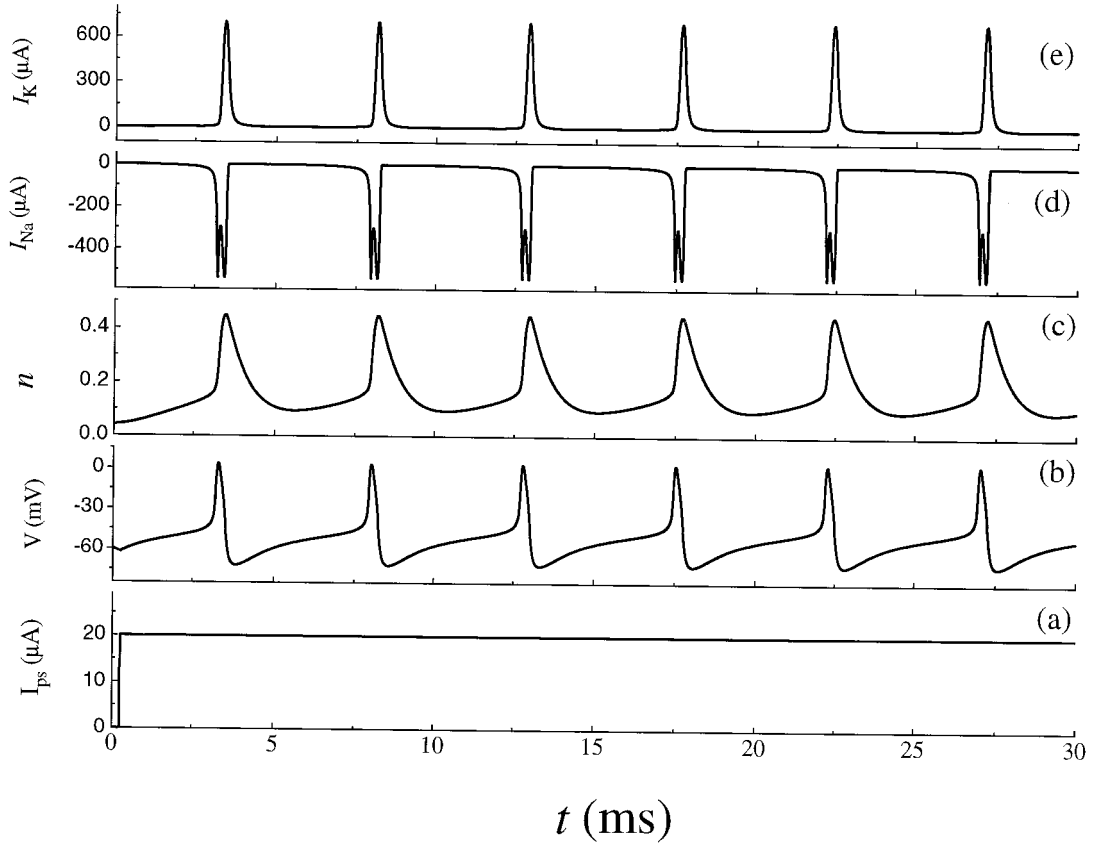

FIGURE 6 The response properties of the afferent model under application of a constant current $I_{ps} = 20\ \mu$A. (*a*) Stimulus; (*b*) membrane potential of the afferent V; (*c*) time-delayed voltage-sensitive gate of K^+ channels; (*d*) inward Na^+ current I_{Na}; (*e*) outward K^+ current I_K.

channels are activated by the depolarization, and the inward Na^+ current increases. This, in turn, accelerates the depolarization of potential V. The increasing potential activates the time-delayed voltage-dependent K^+ channels. The rapidly increasing outward K^+ current suppresses the increase of the potential. Then the potential begins to decrease, which causes the deactivation of Na^+ channels. Because the Na^+ current decreases, the repolarization of the membrane potential is accelerated. The time-delayed voltage-dependent K^+ channels are also deactivated. As a result, the afferent potential approaches the resting state. However, the constant current I_{ps} continuously stimulates the afferent potential, and a new oscillation cycle occurs.

Larger constant current I_{ps} leads to a faster and a larger depolarization process. Larger depolarization, in turn, causes faster repolarization. Thus, the oscillation period and the latency duration between stimulus onset and the occurrence of the first spike in the afferent fiber is shortened by an increase in I_{ps}. The dependence of the oscillation period on the stimulus current is given in Fig. 7. Simulation results show that the oscillation period is 9.2 ms at the threshold current $I_{ps} = 17.86$ μA. The calcium ion current intensity of the excited sensory cell is $\sim$5000–4900 $\mu A/cm^2$. We chose the values of parameters w, θ, and ϵ in Eq. 15 as shown in Table 2 so that the corresponding current I_{ps} that can initiate afferent fiber oscillation is $\sim$22.2–12.0 μA.

Now one can see how the A- and B-receptor models process the information contained in the EOD stimulus. Although the real EOD pulse is very short (duration < 0.5 ms), it can drive the cell to the greatly depolarized state. Due to the large relaxation time constant of free intracellular calcium ions in the submembrane space of the cell, the large calcium ion current is maintained for $\sim$10 ms. As a result, the afferent fiber can oscillate with a duration of $\sim$10 ms. Differently distorted EODs cause differently depolarized potentials and different durations in the A- and B-cells. The release of transmitter at the afferent fiber synapse induced by the various depolarizations then differs in intensity and duration. A higher intensity of transmitter release leads to a shorter spike latency in the afferent fiber. Coincidentally, the longer the duration of transmitter release, the larger the number of spikes.

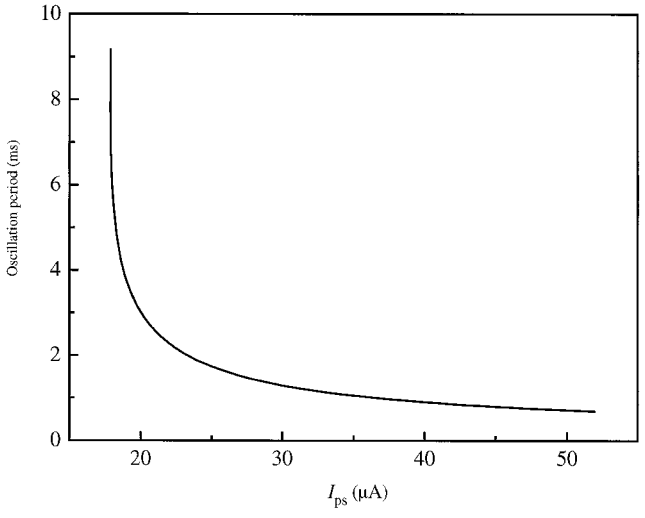

FIGURE 7 The dependence of the oscillation period in the afferent fiber on the stimulus current I_{ps} from 17.8 to 52.0 μA. The oscillation periods decrease from 9.2 to 0.69 ms.

Origin of functional differences between A- and B-receptors

A-receptors are known to respond to the intensity of the EOD. What kind of information can B-receptors process? It is seen from Eq. 5 that the sensory cell not only responds to the EOD intensity V_{stim}, but also senses the variation dV_{stim}/dt of the EOD waveform due to its resistance-capacitance structure. To answer the question, it is a reasonable consideration that A- and B-receptors respond mainly to one of the two terms, respectively.

An object with a considerable capacitive component has two effects on EOD signal (von der Emde, 1990, 1992b). 1) There is a change in the intensity if the impedance of the object differs from that of the surrounding water. The impedance of a capacitive object is frequency-dependent in contrast to that of a resistive object. Low-frequency components of an EOD are attenuated more strongly than high-frequency components. 2) There is a frequency-dependent phase shift of the signal: frequency components within a certain range, depending on the value of the capacitance, are phase-shifted more strongly than others. Objects with no capacitive components do not cause any phase shift of the signal. Both frequency-dependent attenuation and frequency-dependent phase shift can lead to a strong distortion in the waveform of the EOD, i.e., cause a large change in the variation of EOD waveform.

In this subsection we show that because of the difference in morphology of A- and B-cells, and of the differences in the conductance of the leak ion channels of the apical membranes and the membrane capacitance between A- and B-cells, the A-receptor can mainly respond to the intensity of EOD stimulus, while the B-receptor is sensitive to the distortion of the EOD waveform caused by the capacitive component of object.

Anatomical experiments (Szabo and Wersall, 1970; Bell et al., 1989) showed that the apical membrane of the A-cell in contact with the outer sensory chamber is small in area. However, the apical membrane of the B-cell protruding into the inner sensory chamber is quite large in area. For the A-cell, suppose $S_1/S_2 = 1/a$ with $a > 1$ and $C_1 = C_2 = C_A$, then we have the following potential equation

$$\frac{d\Phi_B}{dt} = \frac{1}{(1+a)C_A} \cdot \left[C_A \frac{dV_{stim}}{dt} + g_0 V_{stim} - g_0(\Phi_B + \Phi_0) - aI \right] \tag{17}$$

where $I = I_{Ca} + I_K + I_L$.

Experiments have shown that most of the B-cells protrude into the sensory chamber, and this exposed cell surface is covered with microvilli (Bell et al., 1989). So we suppose $S_1/S_2 = a$ for the B-cell. Due to the microvilli, the physical properties of apical membrane of the B-cell are also different from those of the A-cell. As a result, the capacitance of the membrane is assumed to be smaller than that of the A-cell: $C_1 = C_2 = C_B = C_A/(ab)$ with $a > b > 1$. Furthermore, let the conductance of the leak channel of B-cell be much smaller than that of A-cell: $g_{0(B)} = g_0/a^2$. Then, for B-cell

$$\frac{d\Phi_B}{dt} = \frac{b}{(1+a)C_A} \cdot \left[\frac{aC_A}{b}\frac{dV_{stim}}{dt} + g_0 V_{stim} - g_0(\Phi_B + \Phi_0) - aI\right] \tag{18}$$

Now, using Eqs. 17 and 18, we discuss the origin of the functional difference between A- and B-electroreceptors. With the same potential stimulus V_{stim}, the A-cell actually responds to the signal

$$A_{stim} = \frac{1}{(1+a)C_A}\left(C_A\frac{dV_{stim}}{dt} + g_0 V_{stim}\right) \tag{19}$$

while the B-cell responds to

$$B_{stim} = \frac{b}{(1+a)C_A}\left(\frac{aC_A}{b}\frac{dV_{stim}}{dt} + g_0 V_{stim}\right) \tag{20}$$

Due to the condition $a > b > 1$, a given stimulus has a larger effect upon the B-cell than the A-cell. As a result, the B-cell has a lower threshold than the A-cell.

With suitably chosen values of the parameters a, b, and g_0, it is possible for the A-cell to hold the relation

$$C_A\frac{dV_{stim}}{dt}|_{max} < g_0 V_{stim}|_{max},$$

while for the B-cell

$$\frac{aC_A}{b}\frac{dV_{stim}}{dt}|_{max} > g_0 V_{stim}|_{max}.$$

It results that the A-receptor can be more sensitive to the intensity of the EOD than to the variation of the EOD waveform, whereas the B-receptor is more sensitive to the latter than to the former.

The relationship between the maximum intensity of EOD stimulus and the maximum time variation of EOD

$$V_{stim}|_{max} \sim 1.8 \times 10^{-5} \times \left[\frac{dV_{stim}}{dt}\right]|_{max} \quad \text{(unit: mV)}$$

holds roughly for a natural biphasic EOD (Shuai et al., manuscript in preparation). In order that the model satisfies the relation, we adjust the values of parameters for A-cell to obtain the condition $C_A/g < 1.8 \times 10^{-5}$ s. If we let g_0 be of the order of 1000 μS/cm^2, then C_A must be of the order of 10^{-2} μF/cm^2. For the B-cell, we have $C_B/g_{0(B)} = (a/b)C_A/g_0 < 1.8 \times 10^{-5}$ s. In fact, in order to let the A-receptor respond sensitively to the EOD intensity and let the B-receptor respond sensitively to the variation of the EOD waveform, we require only the fact that the A- and B-cells possess the structure shown in Fig. 1. It has little relation to the detailed dynamics of the sensory cells and the afferent fibers. As a result, the above discussion is rather general.

The parameter values of A- and B-cells given in Table 1 are typical ones that satisfy the conditions mentioned above. By using these values, we have

$$\frac{d\Phi_B}{dt} = \frac{1}{1.1\times 10^{-4}}\left(10^{-5}\frac{dV_{stim}}{dt} + V_{stim} - \Phi_B - \Phi_0 - \frac{1}{300}I\right) \tag{21}$$

for the A-cell. Furthermore, letting $b = 1.2$, then $S_1/S_2 = 10$, $g_{0(B)} = 30$ μS/cm^2, and $C_B = 2.5 \times 10^{-3}$ μF/cm^2 for the B-cell, we obtain

$$\frac{d\Phi_B}{dt} = \frac{1.2}{1.1\times 10^{-4}}\left(\frac{25}{3}\times 10^{-5}\frac{dV_{stim}}{dt} + V_{stim} - \Phi_B - \Phi_0 - \frac{1}{300}I\right) \tag{22}$$

Response to the square waveform stimuli

To investigate experimental response properties of A- and B-receptors, square waves were used as stimuli to the receptors (Bell, 1990; von der Emde and Bleckmann, 1992b). Experimental results show that, for stimulation with outside positive square waves, the maximum numbers of spikes discharged by A-receptors was two to four, whereas the maximum numbers for B-receptors was four to eight spikes. A large increase in the threshold of A- and B-receptors was observed when the duration of the square wave stimuli was decreased from 1.0 to 0.1 ms. The threshold values for different A-receptors varied over a wide range, whereas various B-receptors appeared to have relatively homogeneous thresholds.

Now we consider the origin of these experimental results based on our receptor model. To simulate the transient process during the rising and falling slope of the square wave stimulus, the stimulus should change linearly within a very short time period δt. Then, during the rising or falling slope of the square wave stimulus, the stimulus linearly increases or decreases with a variation of $\pm V_{stim}/\delta t$, respectively, where V_{stim} is the height of the square wave. During the plateau region of the stimulus, its intensity is constant and has the value V_{stim}. If $\delta t \leq 10$ μs, then during the rise and fall of the stimulus the inequality $10^{-5}dV_{stim}/dt > V_{stim}(t)$ holds. Therefore, the B-receptor and the A-receptor respond primarily to the variation of stimulus intensity, as seen from Eq. 19. Positive square waves were used in the experiments (Bell, 1990; von der Emde and Bleckmann,

1992b) to discuss how A- and B-receptors respond to the various intensities of stimuli. Our model implies that it is mainly due to the variation at the onset of the positive square wave, rather than its intensity, that the A-cells as well as the B-cells are depolarized. Therefore, the response properties of the receptors to the square wave stimulus are quite different from those to the natural EOD stimulus, especially for the A-receptor, whose response arises mainly from the stimulus intensity.

Responses of A- and B-receptors to a 10-ms outside positive square wave stimulus are calculated as a function of the stimulus intensity, and are given in Fig. 8. Here $\delta t = 10$ μs is used and the stimulus is applied at $t = 0.25$ ms. For A- and B-receptors, as the stimulus intensity increases, the spike latencies decrease, and additional spikes are added to the response. The threshold stimulus intensity for the A-receptor is 2.83 mV with the spike latency of 4.35 ms. At the stimulus intensity of 9 mV, the first spike latency decreases to 2.69 ms, and the number of spikes becomes 5. For the B-receptor, the threshold value is 1.84 mV with a spike latency of 4.43 ms. At the stimulus intensity of 3.3 mV the first spike latency is 2.63 ms and the number of spikes increases to eight. Fig. 9 shows the latencies of each spike responding to the various stimulus intensities for A- and B-receptors. Here, the latency indicates the time duration between the onset of stimulus and the peak of each spike in the afferent fiber. For the A-receptor, when the stimulus intensity increases from 2.83 to 10.3 mV, the latency of the first spike decreases from 4.35 to 2.65 ms. For the B-receptor, in contrast, the latency of the first spike decreases from 4.43 to 2.62 ms when stimulus intensity increases from 1.84 to 3.32 mV. The variability of the first spike latency is large when the stimulus intensity is a little higher than the threshold, and becomes rapidly small as the stimulus is increased. This is in good agreement with the observed results (Bell, 1990), although the first-spike latency obtained for the threshold intensity is short compared with the experimental results (Bell, 1990).

It has been shown (Bell, 1990) that the time interval between two adjacent spikes increases gradually for the later spikes. This property arises from the following reason. With the onset of the stimulus, the cells are rapidly depolarized. The basal membrane potential approaches its maximum value in a short time interval, then it slowly decreases because of the slow increase of the free intracellular Ca^{2+} in the submembrane space. A similar change is caused for the release of transmitter at the afferent fiber synapse (i.e., I_{ps}). Thus the time intervals between the spikes increase gradually with time, as shown in Fig. 9.

Higher square wave stimulus leads to a larger depolarization of the cell with a longer time duration. This causes the shorter latency of each spike and a higher spike number for the afferent fiber. An increase of duration of the stimulus induces a similar effect. After the depolarization of the cell, the remaining outside positive stimulus always has a lasting depolarization effect on the basal membrane potential of the cell and can delay the return of the cell to the resting attraction region. Thus, although the increase of stimulus duration has little effect upon the latency of the first spike, it affects the following spikes so that the latencies of the following spikes decrease and the spike number increases.

Now we consider the effect of the duration of a square wave stimulus on the threshold of the receptors. The calculated results for the dependence of threshold stimulus intensity on the duration of outside positive square wave stimuli are given in Fig. 10 for A- and B-receptors. There are two typical transition time intervals in the cell when it is depolarized by a stimulus. One is the transition interval of the sensory cell from the resting equilibrium state to the greatly depolarized state just after the onset of the square wave stimulus. This time interval is very short. In our model, it is $\sim$0.3 ms. The second interval is the transition time of the afferent fiber from the onset of transmitter release to the appearance of the first spike. Because of the short transition interval of the sensory cell, the time interval of the afferent almost equals the first spike latency, which is $\sim$4.3 ms. If the duration of the stimulus is so long that its downfall comes after the first spike, the stimulus duration has no effect upon the first spike. Therefore, the threshold does not depend on the duration, as shown in Fig. 10. If the downfall of the stimulus occurs within the transition time interval of the afferent ($\sim$0.3–4.3 ms), the negative variation of the stimulus can rapidly cause the cell to go back to the resting attraction region. In this case, the release of transmitter decreases a little, and then a little stronger stimulus is required to obtain a spike. If the downfall of the stimulus occurs within the transition interval of the cell ($<$0.3 ms), the basal membrane potential of the cell is drawn back to the resting attraction region before the transition to the depolarization state occurs. Then no spikes can be achieved in the A- and B-afferents. Thus, a high intensity of the square wave stimulus is required to depolarize the cell greatly enough to overcome the negative effect of the early downfall of the stimulus.

Experimental results (Bell, 1990) have shown that different A-receptors possess different threshold values distributing over a wide range when they are stimulated with a 10-ms outside positive stimulus, while different B-receptors appear to have relatively homogeneous values of threshold. The microscopic origin of this difference arises from the following property of A- and B-receptors. It seems reasonable for actual A- and B-receptors that the values of parameters included in each receptor vary slightly for every receptor. Therefore, we investigated the effect of slight changes in parameter value on the response property of A- and B-receptors using the present model.

Stimulated by the threshold stimulus, the cell produces the threshold Ca^{2+}-current density I_{Ca}^{thr} and the threshold synaptic current I_{ps}^{thr} that can fire the afferent fiber. Now, if one of the parameters in the cell model changes a little, it usually leads an increase or a decrease of I_{Ca}. To obtain the fixed threshold synaptic current I_{ps}^{thr}, it is required to decrease or increase the stimulus intensity. Then the intensity obtained is the new threshold intensity. From Eqs. 17 and 18

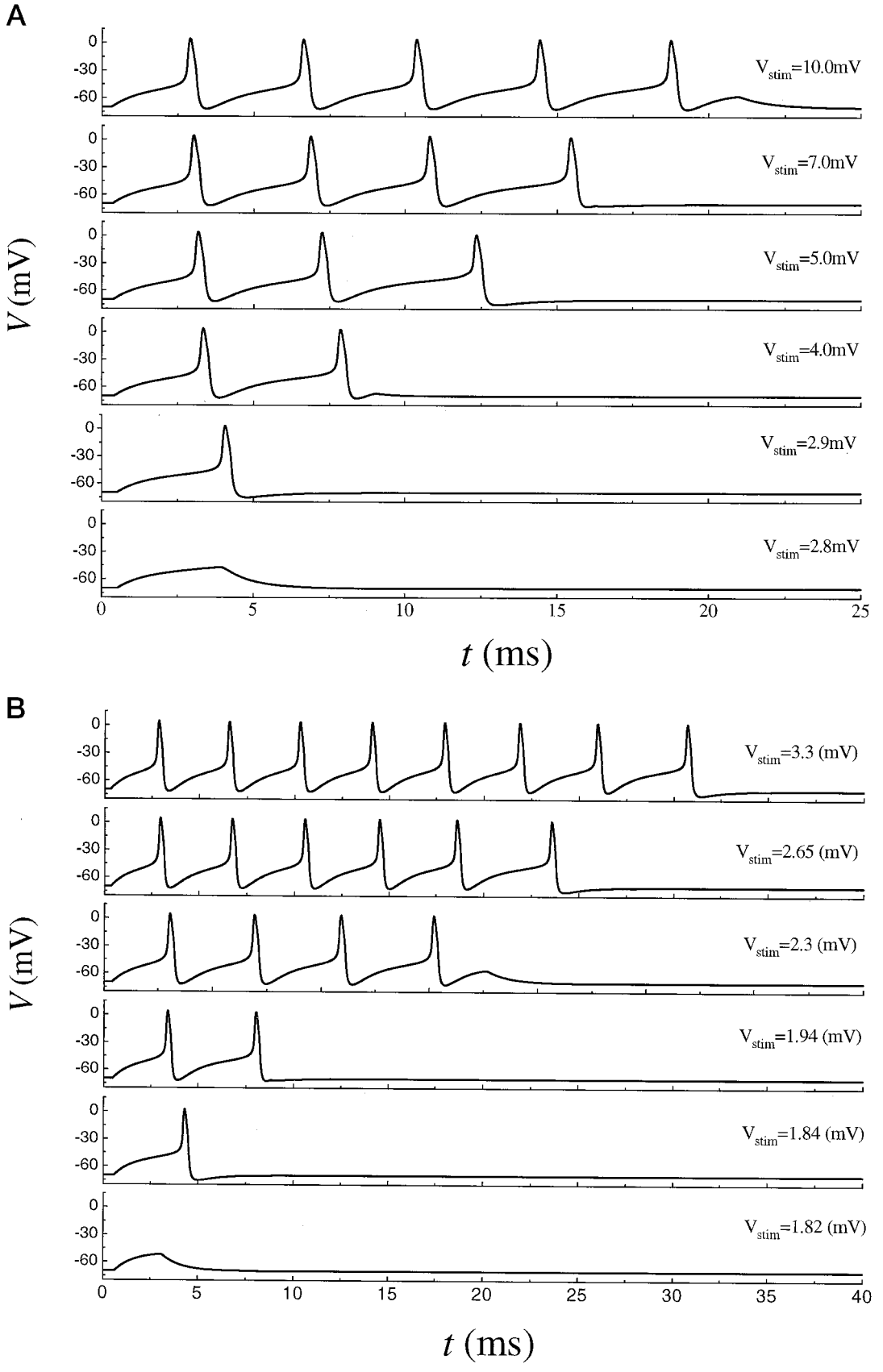

FIGURE 8 The responses of afferent fiber innervating A- and B-cells induced by the 10-ms outside positive square wave stimuli for various stimulus intensities. (*A*) For the A-receptor, the increase in the stimulus intensity above the threshold causes a reduction in latency of the response and an increase in the number of spikes from 1 to 5. (*B*) For the B-receptor, the increase in the stimulus intensity above the threshold causes a reduction in latency of the response and an increase in the number of spikes from 1 to 8.

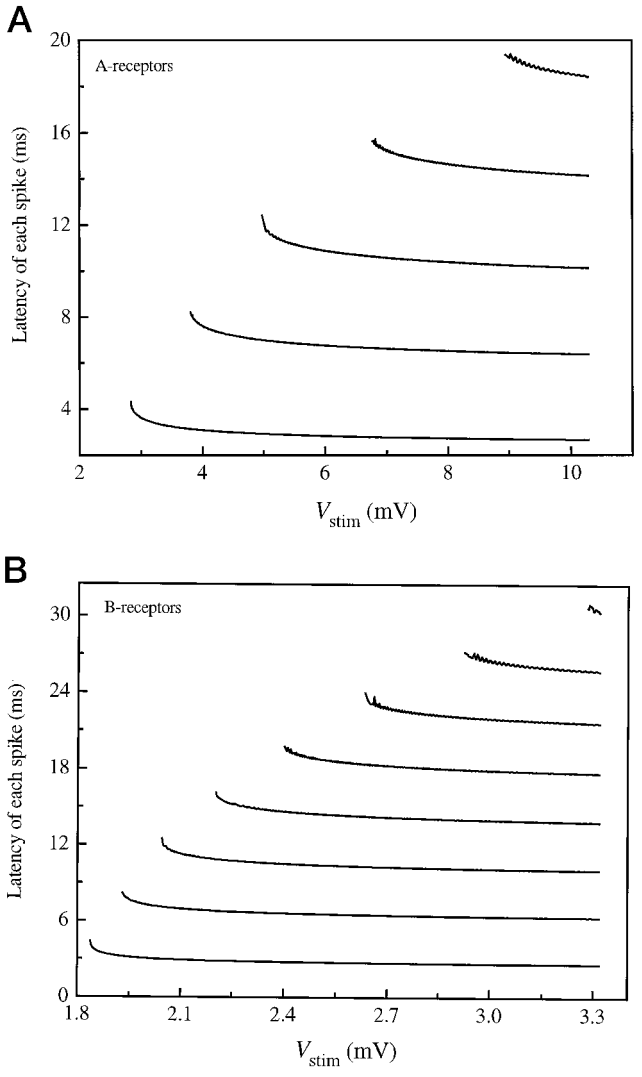

FIGURE 9 The latencies of the first several spikes in A- and B-receptors generated by 10 ms outside positive square stimuli with various intensities. Here, the voltage of the stimulus is shown on the y axis, while latency is shown on the x axis. (*A*) The latencies of five spikes for the A-receptor. (*B*) The latencies of eight spikes for the B-receptor.

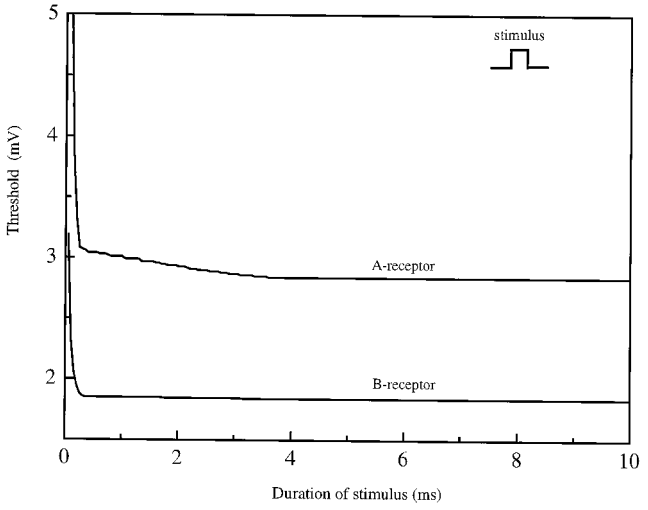

FIGURE 10 The effect of duration of the positive square wave stimuli on the threshold stimulus intensity of A- and B-receptors. The upper line is for the A-receptor, while the lower is for the B-receptor.

one can see that the change of A_{stim} required for the A-receptor is almost equal to that of B_{stim} required for the B-receptor. However, it can be seen from Eqs. 19 and 20 that the equivalent amount of increase in actual signal A_{stim} and B_{stim} requires different amounts of increase in stimulus intensity V_{stim} for A- and B-receptors, respectively. The A-receptor requires a larger increase in stimulus intensity than the B-receptor. For example, the value of the half-maximal activation potential V_τ in Eq. 9 is changed a little around the value 5.6 mV. The simulation shows that, when the value V_τ is changed to 5.61 or 5.59 mV, the threshold value of V_{stim} for the A-receptor changes from 2.83 to 2.77 or 2.90 mV; that is, the changes are ~2.3%; while for B-receptor it changes from 1.84 to 1.83 or 1.85 mV; that is, the changes are ~0.54%. A similar result can be obtained for the change of parameter values in the afferent fiber. For example, the simulation shows that, when the value of synaptic strength ω is changed from 24 to 23 μA or to 25 μA, the threshold for the A-receptor changes to 2.75 or 2.95 mV; that is, the changes are ~2.3%; while for the B-receptor it changes to 1.83 or 1.85 mV; that is, the changes are ~0.54%.

The responses of A- and B-receptors to an outside negative square wave stimulus were also investigated in experiment (Bennett, 1965; Bell, 1990). At first glance, it seems strange that the receptor can be excited by an outside negative stimulus; with such a stimulus the receptor should be hyperpolarized, while in fact it is depolarized. As mentioned above, A- and B-receptors mainly respond to the variation part of square wave stimulus. For an outside negative stimulus, the variation is negative at its onset, while it is positive at its switchoff. The latter variation can depolarize both A- and B-cells. As a result, the responses of A- and B-receptors to outside negative square waves occur at the switchoff, while the responses to outside positive square wave stimuli occur at the onset of stimulus (Bennett, 1965; Bell, 1990).

We investigated the response of the present model to the outside negative square wave stimuli. When the stimulus duration is long enough, A- and B-cells are stabilized in a hyperpolarized state that is very close to the resting equilibrium state. Then the value of the activation threshold becomes almost the same as that for the outside positive stimulus, as it should be (Bell, 1990). By using a stimulus with short duration, the depolarization at the switchoff begins from the deeply hyperpolarized state generated by the onset of the stimulus. As a result, a higher threshold potential is required to depolarize the cell. This has been observed for the B-receptors (Bell, 1990). However, the increase of the threshold potential induced by a short negative square stimulus was not observed for the A-receptors. It seems to

be one of the reasons for the disagreement that the stimulus duration used in the experiment was not short enough.

CONCLUDING REMARKS

To understand how the electrosensory system of the weakly electric fish *G. petersii* distinguishes the object, we presented an electroreceptor model. The model has reasonably explained the microscopic origin of the functional difference between A- and B-receptors. We consider the uniqueness of the present model with respect to the simulation of relevant experimental data. The essential origin of the functional difference in the model comes from the fact that the response sensitivities of the receptor to V_{stim} and to dV_{stim}/dt are different between A- and B-receptors, as shown by Eqs. 19 and 20. The sensitivity for V_{stim} is dominant in the A-receptor, which encodes the amplitude of EOD, whereas that for dV_{stim}/dt is dominant in the B-receptor, which codes the distortion of EOD waveform. This fact is physically reasonable. The sensitivity difference then arises from the different morphologies of A- and B-cells, the different conductance of leak ion channels, and the different capacitance of membranes. The morphology difference has been observed. Although the conductance and capacitance differences are our assumptions, they are quite possible, as described previously. Besides these assumptions, we introduced the phenomenological expressions Eqs. 7 and 9 for the dependence of $[Ca^{2+}]$-activated gate g on $[Ca^{2+}]_{sub}$ and of the relaxation time τ on Φ_B, respectively, based on the reasonable considerations. By using the phenomenological expressions, we reasonably simulated several response properties of A- and B-receptors observed under application of various stimuli with artificial waveforms, as shown in Figs. 5 and 8–10. Furthermore, using the model, we have calculated the response properties of A- and B-receptors under applications of EODs distorted by various resistive and capacitive objects and the phase-shifted EODs. It will be shown in the forthcoming paper that the calculated results are in good agreement with the observed relevant data. Because the present model can simulate essential response properties of A- and B-receptors for various kinds of stimuli, the model seems to be unique.

When we compare the response properties of the present model of electroreceptor units with the experimental data, we must take into account a few differences in the conditions used between the experiment and the calculation. 1) In the experiment, the tip of the stimulus electrode is often positioned very close to the electroreceptor pore in order to deliver an electrical stimulus. The reference electrode is placed on the contralateral side of the fish. The stimulus amplitude is measured at the receptor pore by a saline-agar electrode with reference to an internally placed silver wire electrode. Thus the stimulus intensities are expressed in terms of voltage drops across the skin (Bell, 1990; von der Emde, 1992b). In the present model, however, the stimulus potential is considered as the voltage drop across the A- and B-cells. 2) In the experiment, the spike latencies measured are the sum of two delays (Bell, 1990): the first delay is the period between the onset of the stimulus and the generation of a spike in the afferent fiber, referred as transmission delay; the second is between the generation of a spike in the afferent fiber close to the electroreceptors and the arrival of the spike at the recording site, i.e., the propagation time along the axon. In the simulation, in contrast, the latency indicates the time duration between the stimulus onset and the peak of each spike in the afferent fibers. In addition, there are two obvious morphology differences between our model and the real receptor units. 3) The anatomical experiments show that the A- or B-afferents innervate several A- or B-cells, respectively, whereas the afferent in the model receptor innervates only one sensory cell. 4) The mormyromast organ contains outer and inner sensory chambers. A-receptors are located in the outer chamber and B-receptors are located in the inner chamber. In the model, these structural differences between A- and B-receptors are not considered for simplicity. Therefore, we intended in the present paper to obtain not quantitative but qualitative agreements of the calculated results with the observed results. However, it is enough for us to understand the microscopic origins of the observed response properties of A- and B-receptors.

Kashimori and Kambara (unpublished manuscript) pointed out that the integration of responses of many sensory cells by a single afferent is quite important to encode the modulations of amplitude and phase of stimuli under noisy conditions for the P- and T-receptors of the weakly electric fish *Eigenmannia*. The integration of the outputs of many cells in an electroreceptor organ at a spike initiation zone, located on an afferent fiber close to the cells, brings about a compensation of the incomplete outputs induced by weak stimuli, and also an elimination of large irregular noise included in the outputs caused by noisy stimuli (Peters et al., 1997). In *G. petersii*, the A- or B-afferent also innervates several A- or B-cells. The integration of responses of several cells by the afferent may also play an important role to eliminate various kinds of noises included in the stimulus.

We thank Dr. G. von der Emde for helpful suggestions and discussions about the relations of the model to the experimental results and for critically reading the text. The authors also thank Dr. T. R. Chay for helpful discussions on the model.

REFERENCES

Bastian, J. 1986. Electrolocation: behavior, anatomy, and physiology. *In* Electroreception. T. H. Bullock and W. Heiligenberg, editors. Wiley, New York. 577–612.

Bell, C. C. 1990. Mormyromast electroreceptor organs and their afferent fibers in mormyrid fish. III. Physiological differences between two morphological types of fibers. *J. Neurophysiol.* 63:319–332.

Bell, C. C., H. Zakon, and T. E. Finger. 1989. Mormyromast electroreceptor organs and their afferent fibers in mormyrid fish. I. Morphology. *J. Comp. Neurol.* 286:391–407.

Bennett, M. V. L. 1965. Electroreceptors in mormyrids. *Cold Spring Harbor Symp. Quant. Biol.* 30:245–262.

Chay, T. R. 1985. Chaos in a three-variable model of an excitable cell. *Physica D.* 16:233–242.

Chay, T. R. 1990a. Effect of compartmentalized Ca^{2+} ions on electrical bursting activity of pancreatic β-cells. *Am. J. Physiol.* 258:C955–C965.

Chay, T. R. 1990b. Electrical bursting and intracellular Ca^{2+} oscillations in excitable cell models. *Biol. Cybern.* 63:15–23.

Chay, T. R. 1993. The mechanism of intracellular Ca^{2+} oscillation and electrical bursting in pancreatic β-cells. *Adv. Biophys.* 29:75–103.

Fan, Y. S., and T. R. Chay. 1994. Generation of periodic and chaotic bursting in an excitable cell model. *Biol. Cybern.* 71:417–431.

Hall, C., C. C. Bell, and R. Zelick. 1995. Behavioral evidence of a latency code for stimulus intensity in mormyrid electric fish. *J. Comp. Physiol. A.* 177:29–39.

Heiligenberg, W. 1973. Electrolocation of objects in the electric fish *Eigenmannia. J. Comp. Physiol.* 87:137–164.

Hodgkin, A. L., and A. F. Huxley. 1952. A quantitative description of membrane current and its application to conduction and excitation in nerve. *J. Physiol.* 117:500–544.

Kashimori, Y., M. Goto, and T. Kambara. 1996. Model of P- and T-electroreceptors of weakly electric fish. *Biophys. J.* 70:2513–2526.

Lund, P. E., E. Grapengresser, E. Gylfe, and B. Hellman. 1991. Intracellular ATP mimics GTP-γ-S in generating Ca^{2+} oscillations in pancreatic β-cells. *Biochem. Biophys. Res. Commun.* 177:777–783.

Penner, R., and E. Neher. 1988. The role of calcium in stimulus-secretion coupling in excitable and non-excitable cells. *J. Exp. Biol.* 139:329–345.

Peters, R. C., J. Brans, F. Bretschneider, E. Versteeg, and A. Went. 1997. Converging electroreceptor cells improve sensitivity and tuning. *Neuroscience.* 81:297–301.

Prentki, M., M. C. Glennon, A. P. Thomas, A. P. Morris, F. M. Matschinsky, and B. E. Corkey. 1988. Cell-specific patterns of oscillating free Ca^{2+} in carbamylcholine-stimulated insulinoma cells. *J. Biol. Chem.* 263:11044–11047.

Rorsman, P., and G. Trube. 1986. Calcium current inactivation in an insulin secreting clonal cell line is mediated by both calcium influx and membrane depolarization. *Pflugers Arch.* 414:1–10.

Sanchez, D. Y., and H. H. Zakon. 1990. The effects of postembryonic receptor cell addition on the response properties of electroreceptive afferents. *J. Neurosci.* 10:361–369.

Schwan, H. P. 1963. Determination of biological impedances. *In* Physical Techniques in Biological Research, vol. VI. W. L. Nastuk, editor. Academic Press, New York, London. 323–407.

Szabo, T., and S. Hagiwara. 1967. A latency-change mechanism involved in sensory coding of electric fish (mormyrids). *Physiol. Behav.* 2:331–335.

Szabo, T., and J. Wersall. 1970. Ultrastructure of an electroreceptor (mormyromast) in a mormyrid fish, *Gnathonemus petersii. J. Ultrastruct. Res.* 30:473–490.

Velasco, J. M., and O. H. Petersen. 1987. Voltage-activation of high conductance K^+ channel in the insulin-secreting cell line RINm5F is dependent on local extracellular Ca^{2+} concentration. *Biochim. Biophys. Acta.* 896:305–310.

von der Emde, G. 1990. Discrimination of objects through electrolocation in the weakly electric fish, *Gnathonemus petersii. J. Comp. Physiol.* 167:413–421.

von der Emde, G. 1993. Capacitance discrimination in electrolocating, weakly electric pulse fish. *Naturwissenschasten.* 80:231–233.

von der Emde, G., and C. C. Bell. 1994. Responses of cells in the mormyrid electrosensory lobe to EODs with distorted waveforms: implications for capacitance detection. *J. Comp. Physiol. A.* 175:83–93.

von der Emde, G., and H. Bleckmann. 1992a. Extreme phase sensitivity of afferents which innervate mormyromast electroreceptors. *Naturwissenschasten.* 79:131–133.

von der Emde, G., and H. Bleckmann. 1992b. Differential response of two types of electroreceptive afferents to signal distortions may permit capacitance measurement in a weakly electric fish, *Gnathonemus petersii. J. Comp. Physiol. A.* 171:683–694.

von der Emde, G., and H. Bleckmann. 1997. Waveform tuning of electroreceptor cells in the weakly electric fish, *Gnathonemus petersii. J. Comp. Physiol. A.* 181:511–524.